Astron. Astrophys. 362, 851–864 (2000)

ASTRONOMY AND ASTROPHYSICS

Fitting planes to early-type galaxies: MIST for the determination of the fundamental plane

F. La Barbera[1], **G. Busarello**[2], **and M. Capaccioli**[1,2]

[1] Università Federico II, Napoli, Italy (labarber@na.astro.it)
[2] Osservatorio Astronomico di Capodimonte, via Moiariello 16, 81131 Napoli, Italy

Received 28 June 2000 / Accepted 31 August 2000

Abstract. The present study deals with the problem of deriving the coefficients of the fundamental plane (FP) of early-type galaxies.

We introduce statistical models of the FP and relative fitting methods: the MIST (*Measurement errors and Intrinsic Scatter Three dimensional*) fits[1]. The MIST fits account for the measurement errors on the variables and their correlations as well as for the intrinsic scatter. We show that the lack of a model of the intrinsic scatter of the FP is the origin of the systematic differences between the various fitting methods.

We also address the problem of estimating the uncertainties of the FP coefficients and determine a simple relation between the sample size and the expected accuracy of the coefficients.

The present study leads to define a 'minimum sample size' for a correct estimate of the uncertainties. For $N \widetilde{<} 30$, both theoretical formulae and re-sampling techniques, like the bootstrap, do not give reliable estimates.

The question of the 'universality' of the FP is addressed by applying the MIST fits to ten samples of cluster galaxies. The FP slopes are actually consistent between the different samples, but, due to the large uncertainties, they could also hide significant systematic differences.

The feasibility of the measurement of the possible variations of the FP slopes as a function of redshift is also proved.

Key words: galaxies: fundamental parameters – methods: statistical – galaxies: clusters: general

1. Introduction

The fundamental plane (FP) is a bivariate relation between observed global properties of early-type (E) galaxies like the effective radius r_e, the mean surface brightness μ_e, and the central velocity dispersion σ_0 (e.g. Dressler et al. 1987, Djorgovski & Davis 1987) of the form[2]:

$$\log r_{\rm e} = a \log \sigma_0 + b\mu_{\rm e} + c \, . \quad (1)$$

The main features of the FP are its small scatter ($\sim 10\%$ in r_e, of the same order of the measurement errors) and the 'tilt' of its slopes with respect to the prediction of the virial theorem for a family of homologous systems with constant M/L ratio.

It is generally believed that the 'tilt' carries information on the nature of Es, although no convincing interpretation has been found that can be reconciled with the small scatter (see e.g. Ciotti et al. 1996, Renzini & Ciotti 1993). It is now clear that part of the 'tilt' is due to the intrinsic non-homology, both structural and dynamical, of the E family (see e.g. Busarello et al. 1997, Graham & Colless 1996, Prugniel & Simien 1997 and references therein). Stellar population effects (e.g. systematic differences in age/metallicity and interstellar matter content) should account for the remaining tilt (see e.g. Mobasher et al. 1999). In that case, the tilt should decrease when moving to near-infrared wavelengths, where these effects are minimized: some evidences exist that this is actually the case (e.g. Pahre et al. 1998, Scodeggio et al. 1998 and references therein). The wavelength dependence of the FP enters also in the comparisons between FP determinations at different redshifts, where different rest-frame wavebands are sampled.

The FP has been soon recognized as a precise tool for distance determinations (e.g. Dressler et al. 1987, Hudson et al. 1997) and, more recently, for constraining cosmological parameters and for studying galaxy evolution (van Dokkum& Franx 1996, Bender et al. 1998, Jørgensen et al. 1999, Kelson et al. 2000, and references therein).

All the above applications are based on comparisons between different determinations of the FP: e.g. different samples, different wavebands, and different redshifts. The method used to derive the FP coefficients and the relative uncertainties play therefore a central rôle for a proper use of the FP.

The determination of the FP requires considerable observational and data analysis efforts (see e.g. Ziegler & Bender 1997 and Ziegler et al. 1999), it is thus desirable that a similar effort be made for the derivation of the coefficients of the FP and for an accurate estimate of the relative uncertainties.

There is still no agreement in the scientific community about the fitting method to adopt. This is partly due to the numerous applications for which the FP is derived (see above), but it also originates from two important points: (1) the measurement errors on the FP variables are comparable (see e.g. Smith

Send offprint requests to: G. Busarello (gianni@na.astro.it)

[1] The FORTRAN codes of the MIST algorithms are available on request to the authors.

[2] This representation of the FP is adopted throughout the paper.

et al. 1997, hereafter SLH97) and correlated (see Jørgensen et al. 1995a, hereafter JFK95a), (2) the scatter around the plane is not completely accounted for by the measurement uncertainties but has also an intrinsic origin (see e.g. Jørgensen et al. 1996, hereafter JFK96).

In the present work we address the problems relative to: (I) the choice of the procedure to derive the FP coefficients (Sect. 2) and (II) techniques to estimate the corresponding uncertainties (Sect. 3).

Starting from the bi-dimensional models introduced by Akritas & Bershady (1996, hereafter AkB96), we propose in Sect. 2.1 statistical models of the FP that account for the various sources of scatter on the variables and derive the relative fitting procedures: the MIST (*Measurement errors and Intrinsic Scatter Three dimensional*) fits.

We then discuss in Sect. 2.2 the capability of the fitting procedures to derive the coefficients of the FP.

Sect. 3 deals with the uncertainties of the coefficients of the FP. The simulation algorithm used for the present analysis is described in Sect. 3.1. In Sect. 3.2 the different methods to estimate the uncertainties are analyzed and compared to the results of the simulations.

The results and the techniques developed in Sects. 2, 3, are applied in Sect. 4 to the comparison of the FPs of different clusters of galaxies.

2. Deriving the FP

The choice of the best fitting procedure in the study of astronomical data is generally a not trivial question: the appropriate method should be always suggested by the scientific problem to be analyzed (see the discussion in Isobe et al. 1990, hereafter IFA90).

The derivation of the FP is usually based on least squares methods: the ordinary least squares (OLS) fits (e.g. Lucey et al. 1991, Kjærgaard et al. 1993, Hudson et al. 1997), in which the root mean square (rms) of residuals relative to one of the variables is minimized, the orthogonal least squares (ORLS) fit (e.g. Busarello et al. 1997), in which it is minimized the rms of residuals perpendicular to the plane, and other methods derived from the previous ones, as the bisector fit (e.g. Graham & Colless 1996) and the arithmetic mean of the OLS coefficients (e.g. Faber et al. 1987). To reduce the effect of outliers, the fits are often performed by robust procedures, in which the sum of absolute residuals is minimized (see JFK96).

Fitting methods based on multivariate analysis techniques, like the principal component analysis (e.g. Bender et al. 1992), have been sometimes adopted. By their nature, however, these methods are not suitable for the determination of best-fit coefficients, so that they will be not considered in the following.

The most natural interpretation of the FP is in terms of a 'mean relation' between global quantities of E galaxies with respect to which they scatter in the space of the observed properties. Drawing hint from AkB96, we will take this interpretation into mathematical terms, by introducing a statistical model for the FP (Sect. 2.1). The corresponding fitting procedures will be also derived.

We will then discuss (Sect. 2.2) the problem of recovering the mean relation and illustrate the origin of the dependence of the FP coefficients on the fitting method.

2.1. A statistical model: the MIST fits

Let us introduce three random variables $\{X_i\}_{i=1,2,3}$, describing the distribution of global quantities of E galaxies. We will assume that $\{X_i\}$ verify the following identity:

$$X_3 = \alpha X_1 + \beta X_2 + \gamma \tag{2}$$

where α and β are the slopes and γ is the zero point of the mean relation.

In the following, we will use capitals to indicate random variables (RV) and the corresponding small letters for their outputs. Given two RVs A and B, we will indicate with $\mathrm{C}(A,B)$ their covariance, with $\mathrm{V}(A)$ and $\mathrm{V}(B)$ their variances and with $\mathrm{E}(A)$ and $\mathrm{E}(B)$ their expected values. The estimators of a given quantity (i.e. the RVs used to approximate the quantity we look for) will be marked with a caret (e.g. $\hat{\alpha}$, $\hat{\beta}$ and $\hat{\gamma}$). An estimator will be said 'unbiased' if its expected value coincides with the quantity to be estimated.

In modeling the scatter around the plane defined by Eq. (2), we have not only to consider measurement errors on the variables but also an intrinsic dispersion.

To this aim, let us introduce two sets of RVs, $\{\Phi_{\mathrm{s}i}\}_{i=1,2,3}$ and $\{\Phi_{\mathrm{m}i}\}_{i=1,2,3}$, with zero expected values, that describe respectively the intrinsic dispersion and the scatter due to measurement errors, and let us consider the following relations:

$$Y_i = X_i + \Phi_{\mathrm{m}i} + \Phi_{\mathrm{s}i} \tag{3}$$

where $\{Y_i\}_{i=1,2,3}$ are the RVs that describe the distribution of the observed quantities of E galaxies (e.g. $Y_1 = \log r_{\mathrm{e}}$, $Y_2 = \mu_{\mathrm{e}}$, $Y_3 = \log \sigma_0$).

The problem is then to determine unbiased estimators of α, β and γ.

From Eq. (2), one obtains the following identities:

$$\mathrm{E}(X_3) = \alpha \cdot \mathrm{E}(X_1) + \beta \cdot \mathrm{E}(X_2) + \gamma \tag{4}$$

$$\begin{aligned}\mathrm{C}(X_2,X_3) &= \alpha \cdot \mathrm{C}(X_1,X_2) + \beta \cdot \mathrm{C}(X_2,X_2) = \\ &= \alpha \cdot \mathrm{C}(X_1,X_2) + \beta \cdot \mathrm{V}(X_2)\end{aligned} \tag{5}$$

$$\begin{aligned}\mathrm{C}(X_1,X_3) &= \alpha \cdot \mathrm{C}(X_1,X_1) + \beta \cdot \mathrm{C}(X_1,X_2) = \\ &= \alpha \cdot \mathrm{V}(X_1) + \beta \cdot \mathrm{C}(X_1,X_2)\end{aligned} \tag{6}$$

where $\mathrm{C}(X_i,X_j)$ and $\mathrm{V}(X_k)$ are the components of the covariance matrix (CM) of $\{X_i\}$. Assuming that $\{X_i\}$, $\{\Phi_{\mathrm{m}i}\}$ and $\{\Phi_{\mathrm{s}i}\}$ are mutually not correlated (hereafter 'hypothesis $\mathcal{H}_1$') and making use of Eqs. (2) and (3), we can express the first and second order moments of $\{X_i\}$ as (see App. A for a straight demonstration and compare AkB96):

$$\mathrm{E}(Y_i) = \mathrm{E}(X_i) \tag{7}$$

$$\mathrm{V}(Y_i) = \mathrm{V}(X_i) + \mathrm{V}(\Phi_{\mathrm{m}i}) + \mathrm{V}(\Phi_{\mathrm{s}i}) \tag{8}$$

$$\mathrm{C}(Y_i,Y_j) = \mathrm{C}(X_i,X_j) + \mathrm{C}(\Phi_{\mathrm{m}i},\Phi_{\mathrm{m}j}) + \mathrm{C}(\Phi_{\mathrm{s}i},\Phi_{\mathrm{s}j}) \tag{9}$$

Eliminating $\mathrm{C}(X_i, X_j)$ and $\mathrm{E}(X_i)$ from Eqs. (4–6) by means of Eqs. (7–9), we obtain a linear system of three equations in α, β and γ, whose solution is:

$$\begin{aligned}\alpha \;=\; & \Delta^{-1} \cdot [\mathrm{C}(Y_2, Y_3) - \mathrm{C}(\Phi_{\mathrm{m}2}, \Phi_{\mathrm{m}3}) - \mathrm{C}(\Phi_{\mathrm{s}2}, \Phi_{\mathrm{s}3})] \cdot \\ & \cdot [\mathrm{C}(Y_1, Y_2) - \mathrm{C}(\Phi_{\mathrm{m}1}, \Phi_{\mathrm{m}2}) - \mathrm{C}(\Phi_{\mathrm{s}1}, \Phi_{\mathrm{s}2})] + \\ - \; & \Delta^{-1} \cdot [\mathrm{C}(Y_1, Y_3) - \mathrm{C}(\Phi_{\mathrm{m}1}, \Phi_{\mathrm{m}3}) - \mathrm{C}(\Phi_{\mathrm{s}1}, \Phi_{\mathrm{s}3})] \cdot \\ & \cdot [\mathrm{V}(Y_2) - \mathrm{V}(\Phi_{\mathrm{m}2}) - \mathrm{V}(\Phi_{\mathrm{s}2})] \end{aligned} \tag{10}$$

$$\begin{aligned}\beta \;=\; & \Delta^{-1} \cdot [\mathrm{C}(Y_1, Y_2) - \mathrm{C}(\Phi_{\mathrm{m}1}, \Phi_{\mathrm{m}2}) - \mathrm{C}(\Phi_{\mathrm{s}1}, \Phi_{\mathrm{s}2})] \cdot \\ & \cdot [\mathrm{C}(Y_1, Y_3) - \mathrm{C}(\Phi_{\mathrm{m}1}, \Phi_{\mathrm{m}3}) - \mathrm{C}(\Phi_{\mathrm{s}1}, \Phi_{\mathrm{s}3})] + \\ - \; & \Delta^{-1} \cdot [\mathrm{C}(Y_2, Y_3) - \mathrm{C}(\Phi_{\mathrm{m}2}, \Phi_{\mathrm{m}3}) - \mathrm{C}(\Phi_{\mathrm{s}2}, \Phi_{\mathrm{s}3})] \cdot \\ & \cdot [\mathrm{V}(Y_1) - \mathrm{V}(\Phi_{\mathrm{m}1}) - \mathrm{V}(\Phi_{\mathrm{s}1})] \end{aligned} \tag{11}$$

$$\gamma \;=\; \mathrm{E}(Y_3) - \alpha \mathrm{E}(Y_1) - \beta \mathrm{E}(Y_2) \tag{12}$$

where we put:

$$\begin{aligned}\Delta \;=\; & [\mathrm{C}(Y_1, Y_2) - \mathrm{C}(\Phi_{\mathrm{m}1}, \Phi_{\mathrm{m}2}) - \mathrm{C}(\Phi_{\mathrm{s}1}, \Phi_{\mathrm{s}2})]^2 + \\ - \; & [\mathrm{V}(Y_1) - \mathrm{V}(\Phi_{\mathrm{m}1}) - \mathrm{V}(\Phi_{\mathrm{s}1})] \cdot \\ \cdot \; & [\mathrm{V}(Y_2) - \mathrm{V}(\Phi_{\mathrm{m}2}) - \mathrm{V}(\Phi_{\mathrm{s}2})] \end{aligned} \tag{13}$$

On increasing the sample size, the expressions obtained by substituting in the previous equations the terms $\mathrm{C}(Y_i, Y_j)$ with their unbiased estimates $\hat{\mathrm{C}}(Y_i, Y_j)$ (hereafter $\hat{\alpha}$, $\hat{\beta}$ and $\hat{\gamma}$), will approximate more and more closely the 'true coefficients' α, β and γ. The quantities $\hat{\alpha}$, $\hat{\beta}$ and $\hat{\gamma}$ will thus furnish unbiased, asymptotically normal, estimates of α, β and γ. In App. B the analytical formulae of the relative CM components are also derived.

If $\{Y_i\}$ are normally distributed, the unbiased estimators for the moments of $\{Y_i\}$ are defined by the following usual expressions:

$$\hat{\mathrm{E}}(Y_j) \;=\; \frac{1}{N} \cdot \sum_{i=1,N} y_{j_i} \tag{14}$$

$$\hat{\mathrm{V}}(Y_j) \;=\; \frac{1}{N-1} \cdot \sum_{i=1,N} \left(y_{j_i} - \overline{Y_j}\right)^2 \tag{15}$$

$$\hat{\mathrm{C}}(Y_j, Y_k) \;=\; \frac{1}{N-1} \cdot \sum_{i=1,N} \left(y_{j_i} - \overline{Y_j}\right) \cdot \left(y_{k_i} - \overline{Y_k}\right) \tag{16}$$

The fitting procedure based on Eqs. (10–13) and (14–16) will be indicated hereafter by the acronyms $MIST$, *Measurement errors and Intrinsic Scatter Three dimensional* fit.

2.2. Deriving the coefficients of the FP

To discuss the application of Eqs. (10–16) to the derivation of the FP, it is important to remark the following points:

$\mathcal{R}_1$. The terms $\mathrm{V}(\Phi_{\mathrm{s}3})$ and $\mathrm{V}(\Phi_{\mathrm{m}3})$ do not appear in Eqs. (10–13). The estimators of α, β and γ are therefore independent of the scatter along the dependent variable.

$\mathcal{R}_2$. Setting equal to zero the other components of the CMs of $\{\Phi_{\mathrm{m}i}\}$ and $\{\Phi_{\mathrm{s}i}\}$ in Eqs. (10–13) and using Eqs. (14–16), we obtain exactly the expressions of the OLS_{Y_3} estimators, where the subscript Y_3 is used to indicate the dependent variable in the fit[3]. If, on the other hand, every variable is affected by dispersion, the quantities $\mathrm{C}(Y_1, Y_2)$ would give a biased estimate of $\mathrm{C}(X_1, X_2)$ as shown by Eqs. (5, 6). To correct for the bias the CM components of $\{\Phi_{\mathrm{m}i}\}$ and $\{\Phi_{\mathrm{s}i}\}$ are needed (see AkB96).

$\mathcal{R}_3$. As follows from $\mathcal{R}_1$ and $\mathcal{R}_2$, to recover the mean relation by Eqs. (10–13) we have altogether ten degrees of freedom, given by five elements of the CMs of $\{\Phi_{\mathrm{m}i}\}$ and $\{\Phi_{\mathrm{s}i}\}$ respectively.

$\mathcal{R}_4$. Since Eqs. 3 have the same dependency on the three variables, *the best-fit coefficients obtained by means of Eqs. (10–13) are independent of the choice of the dependent variable*.

$\mathcal{R}_5$. New unbiased estimators of the coefficients in Eq. (2) can be defined by taking some average of the slopes of the three planes determined by Eqs. (10–13) using each of the $\{Y_i\}$ as dependent variable. We can define a *bisector plane* (see also Graham & Colless 1996), whose slopes are given by the vectorial sum of the normal vectors to the three planes obtained by Eqs. (10–13), and whose zero point is obtained by Eq. (12). The advantage of the 'bisector' fit (hereafter $\mathrm{MIST}_{\mathrm{BIS}}$ fit) consists in the larger effectiveness (i.e. smaller variances for given sample size) of the relative estimators (see Sect. 3.2, and IFA90 for the two-dimensional case).

$\mathcal{R}_6$. There are often large systematic in-homogeneities between different samples of data, due to differences in the procedures adopted to derive them (see e.g. Smith et al. 1997). To account for such in-homogeneities, the least squares fits (ORLS and OLS) are often performed using robust estimators. The robust statistics can also be implemented to the MIST regression, by using robust estimators for the moments of $\{Y_i\}$ in Eqs. (10–13).

From the derivation of the equations in the previous section, it follows that, in order to recover the coefficients of the mean relation, α, β and γ, some requests must be satisfied:

$\mathcal{H}_1$: $\{X_i\}$, $\{\Phi_{\mathrm{m}i}\}$ and $\{\Phi_{\mathrm{s}i}\}$ are not mutually correlated;
$\mathcal{H}_2$: estimates of the CM components of $\{\Phi_{\mathrm{m}i}\}$ are known;
$\mathcal{H}_3$: estimates of the CM components of $\{\Phi_{\mathrm{s}i}\}$ are available;
$\mathcal{H}_4$: unbiased estimates of the CM components of $\{Y_i\}$ are known.

The hypothesis $\mathcal{H}_1$ is practically equivalent to assume that the measurement errors and the intrinsic scatter on the FP variables do not depend on the 'location' on the FP. This is not the case for the measurement uncertainties on the observed parameters and, *a priori*, it could be not true even for the intrinsic dispersion. However Eqs. (8–13) continue to be valid by simply substituting the CM components of $\{\Phi_{\mathrm{m}i}\}$ and $\{\Phi_{\mathrm{s}i}\}$ with their expected values as a function of the 'position' on the plane (see App. A and B for details).

[3] The OLS method can be thus regarded, in this respect, as a particular case of the MIST fit, in which the scatter is completely ascribed to the direction of the dependent variable.

Concerning the measurement uncertainties (hypothesis $\mathcal{H}_2$), Eqs. (10–13) can still be used by adopting averaged values of $\mathrm{C}(\Phi_{\mathrm{m}i},\Phi_{\mathrm{m}j})$. To this aim, we suggest to proceed as follows. The quantities $\mathrm{V}(\Phi_{\mathrm{m}i})$ can be estimated as the square of the mean error[4] on the parameters $\mathrm{Y_{mi}}$. For what concerns $\mathrm{C}(\Phi_{\mathrm{m}i},\Phi_{\mathrm{m}j})$, the only term that does not vanish, is $\mathrm{C}(\log r_{\mathrm{e}},\mu_{\mathrm{e}})$ due to the correlation between the uncertainties in $\log r_{\mathrm{e}}$ and μ_{e}. The quantities $\mathrm{C}(\Phi_{\mathrm{m}i},\Phi_{\mathrm{m}j})$ are never given in literature, so that one is forced to make some approximations. Since $\Delta\log r_{\mathrm{e}} \approx \alpha{\cdot}\Delta\mu_{\mathrm{e}}$ with $\alpha \approx 0.3$ (see JFK96), we can set $\mathrm{C}(\log r_{\mathrm{e}},\mu_{\mathrm{e}}) \approx \alpha{\cdot}\mathrm{V}(\mu_{\mathrm{e}})$. The uncertainties introduced by this approximation will be discussed in Sect. 4.

Assumptions $\mathcal{H}_3$ and $\mathcal{H}_4$, cannot be satisfied because we do not have a physical model of the probability distribution of E galaxies in the space of the observed quantities. It is thus necessary to introduce some simplifying assumptions:

$\mathcal{H}'_3$: on the basis of $\mathcal{R}_1$ we can only assign all the intrinsic dispersion to the dependent variable.

$\mathcal{H}'_4$: the only possible simple assumption is that $\{Y_i\}$ are normally distributed (see Eqs. 14–16).

Both these assumptions introduce a 'bias' in the estimate of α, β and γ, so that *the coefficients a, b and c in Eq. (1) do not necessarily coincide with α, β and γ*. Moreover, because of $\mathcal{H}'_3$, the estimates obtained by Eqs. (10–13) with a different choice of the dependent variable do not correspond to the same statistical model and so do not define the same plane.

In order to better understand the bias introduced by $\mathcal{H}'_3$ and $\mathcal{H}'_4$, we used numerical simulations of the FP. The simulations were constructed giving a scatter around the plane in the $\log\sigma_0$ direction by a normal RV (see Sect. 3.1 for details). The variance of $\log\sigma_0$ has been varied in the range of values obtained for the $\log\sigma_0$ scatter of different samples of galaxies (see Sect. 4.1). The FP coefficients have been derived for each simulation by the MIST fits, with assumptions $\mathcal{H}'_3$ and $\mathcal{H}'_4$, using each of $\{Y_i\}$ as the dependent variable (hereafter MIST_{Y_i} fits), and by the $\mathrm{MIST_{BIS}}$. We used the estimates of $\mathrm{C}(\Phi_{\mathrm{mi}},\Phi_{\mathrm{mj}})$ obtained by typical values of the uncertainties on FP parameters (0.03 in $\log r_{\mathrm{e}}$, 0.1 in μ_{e} and 0.03 in $\log\sigma_0$).

In Fig. 1, we plot the coefficient a against $\sigma^2_{\log\sigma_0}$ (similar results are obtained for b and c). The values of the FP coefficients obtained by the various fitting methods turn out to be systematically different, by an amount that increases with the scatter. An estimate of this difference for the MIST fits will be given in Sect. 4 by comparing the FPs of different clusters of galaxies.

The assumption $\mathcal{H}'_4$ introduces likely the same amount of bias in the various fits. To illustrate this point, let us consider an example in which the CM components of the intrinsic dispersion are 'known'. We will assume $\mathrm{V}(\Phi_{\mathrm{m}\log\sigma_0}) + \mathrm{V}(\Phi_{\mathrm{s}\log\sigma_0}) = \mathrm{V}(\Phi_{\mathrm{m}\log\mathrm{r_e}}) + \mathrm{V}(\Phi_{\mathrm{s}\log\mathrm{r_e}}) = 0.0035$ (a scatter of $\sim 14\%$ in $\mathrm{r_e}$ and σ_0)[5] and that the other CM terms of $\{\Phi_{\mathrm{m}i}\}$ and $\{\Phi_{\mathrm{s}i}\}$ vanish. We now create a FP simulation, and derive a, b and c by the MIST fits, using the assigned values of the CM components of $\{\Phi_{\mathrm{s}i}\}$ and $\{\Phi_{\mathrm{m}i}\}$, and making therefore *only* the hypothesis $\mathcal{H}'_4$. The results of the fits are shown in Table 1: the FP coefficients are practically independent of the fitting method.

We then conclude that the differences of Fig. 1 are due only to the assumption $\mathcal{H}'_3$: *the lack of a model for the intrinsic dispersion of the FP variables is thus at the origin of the dependency of the FP coefficients on the fitting procedure*. The larger is the scatter around the plane, the larger will be the bias due to the fitting method.

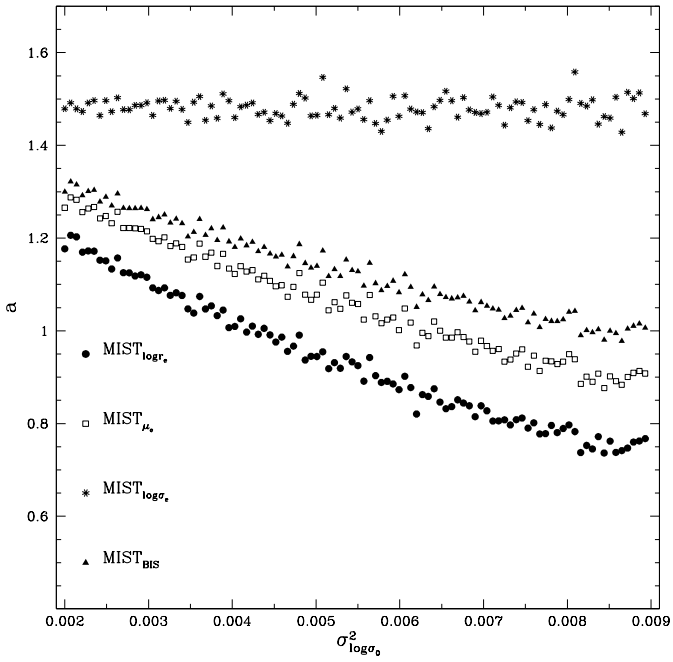

Fig. 1. Coefficient a of FP simulations against the $\log\sigma_0$ variance, $\sigma^2_{\log\sigma_0}$. The size of the simulations is $N = 3000$. The symbols correspond to different fitting methods as shown in the lower left.

Table 1. Values of a, b and c of a FP simulation with intrinsic dispersion 'known' (see text). The sample size is $N = 3000$. Column 1: FP coefficients a, b and c. Columns 2, 3, 4 and 5: values obtained by the different MIST fits (see subscripts in the top row) with corresponding uncertainties (1σ intervals).

	$\mathrm{logr_e}$	μ_{e}	$\mathrm{log}\sigma_0$	BIS
a	1.26 ± 0.02	1.28 ± 0.02	1.28 ± 0.01	1.28 ± 0.01
b	0.310 ± 0.002	0.308 ± 0.002	0.309 ± 0.002	0.309 ± 0.002
c	-8.27 ± 0.07	-8.23 ± 0.07	-8.20 ± 0.07	-8.24 ± 0.06

3. Uncertainties on the FP coefficients

Two kinds of methods are usually adopted to estimate the uncertainties on fit coefficients: theoretical methods and re-sampling techniques.

The 'theoretical uncertainties' are obtained from the analytical expression of the variances of the estimators (e.g. IFA90

[4] Notice that the mean errors are often the only significant available estimates.

[5] This amounts to a 15% scatter in the σ_0 direction, i.e. to the mean value of the FP scatter of clusters, see Sect. 4.

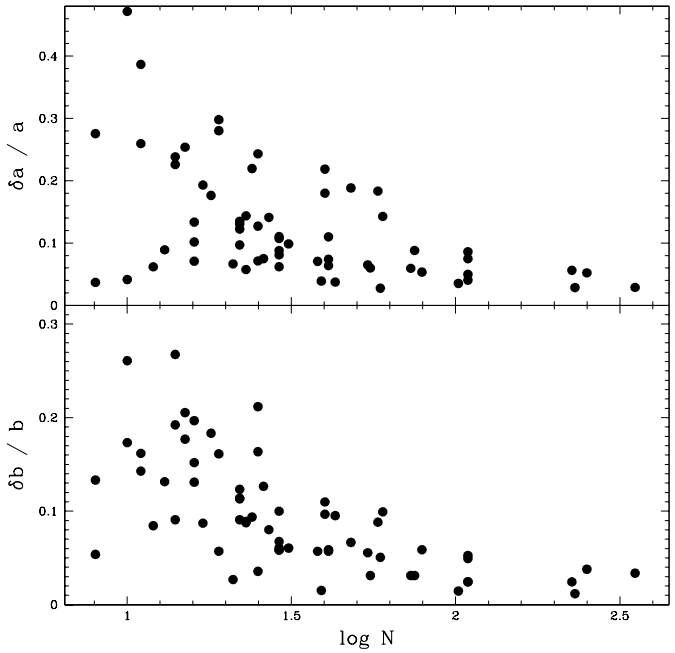

Fig. 2. Relative uncertainties $\delta a/a$ and $\delta b/b$ on FP slopes against the sample size (see text). The values are drawn from literature. Sources of the uncertainties and relative sample sizes (within square brackets): Busarello et al. (1997) [40]; de Carvalho & Djorgovski (1992) [31 40 55 58]; D'Onofrio et al. (1997) [25]; Dressler et al. (1987) [43]; Graham (1998) [7 18 25 25]; Graham & Colless (1996) [26]; Hudson et al. (1997) [352]; Jørgensen et al. (1996) [79 22 24 14 10 14 29 8 19 226 109 109 109 109 41 41]; Mobasher et al. (1999) [48]; Pahre et al. (1995) [8 10 12 13 16 59]; Pahre et al. (1998) [251 60 16 23 15 14 15 17 11 19 11 27]; Prugniel & Simien (1994) [102]; Prugniel & Simien (1996) [231 39 21]; Recillas-Cruz et al. (1990) [29 29 29]; Recillas-Cruz et al. (1991) [22 22 22]; Scodeggio et al. (1998) [38 41 54 75 73 29].

and Feigelson & Babu 1992). By their nature, these estimates are valid only asymptotically, i.e. for large sample sizes.

When analytical formulae are not available, or when the sample is small, re-sampling procedures are adopted. The statistics of interest is calculated for various 'pseudo-samples' drawn from the original data set. The uncertainties are then derived from the distribution of pseudo-values. The main re-sampling procedures are known as 'jackknife' (see Quenouille 1949 and Tukey 1958) and 'bootstrap' (see Efron 1979 and Efron & Tibshirani 1986). In the jackknife, one point is extracted in sequence from the original data set, so that a number of pseudo-samples equal to the sample size is constructed. In the bootstrap, random samples are drawn by replacement from the actual data set.

Fig. 2 shows the relative uncertainties on the FP coefficients a and b, as drawn from literature, as a function of the sample size N. *The large scatter of the values of the uncertainties is indicative of the inconsistency between the methods used in the different works to estimate the errors*.

In the following we will analyze the performance of the methods to estimate the FP uncertainties with special regard to the rôle of the sample size. The analysis will be performed by numerical simulations, which are described in the next section.

3.1. The simulation algorithm

The simulations consist in distributions of points extracted from a common 'parent distribution'. To derive the parent population we based on the distribution in the parametric space of the galaxies in the Coma cluster (hereafter the 'template' sample). This choice is mandatory since Coma is the only cluster with FP parameters available for a large number of galaxies.

The simulation algorithm consists in the following.

- At first, we derived a parent distribution of E galaxies in the plane ($\mu_{\rm e}$,$\log r_{\rm e}$), using the photometric data in the Gunn r band by JFK95a for 146 galaxies in Coma. The sample is complete out to Gunn $\mathrm{r} \simeq 15.5$ mag. The distribution with respect to $\mu_{\rm e}$ was described by a normal RV. The $\mu_{\rm e}$ interval of the template was binned, and the mean value (MV) and standard deviation (SD) of the $\log r_{\rm e}$ distribution derived for each bin. The MVs and the SDs were then fitted with respect to the central values of $\mu_{\rm e}$ by polynomials of suitable order, and the best-fit curves were used to interpolate a value (and a scatter) of $\log r_{\rm e}$ to each value of $\mu_{\rm e}$.
- Using σ_0 by Jørgensen et al. (1995b, hereafter JFK95b) for 75 galaxies of the photometric sample (see Sect. 4), we determined the FP coefficients and the root mean square (rms) of $\log \sigma_0$ residuals, $s_{log\sigma_0}$, by the $\mathrm{OLS}_{\log \sigma_0}$ fit. We found $a \simeq 1.50$, $b \simeq 0.328$, $c \simeq -9.1$ and $s_{log\sigma_0} \simeq 0.048$. These quantities were used to assign to the points a value and a scatter with respect to the variable $\log \sigma_0$.

One of the simulated samples is compared to the template in Fig. 3, to show how the simulations resemble very well the distribution of Coma galaxies.

3.2. Estimating the uncertainties

We derived the 'true uncertainties' on the FP coefficients as a function of the sample size in the following way.

FP simulations of fixed size N were constructed and the coefficients a, b and c determined for each sample. The 'true uncertainties', δa, δb and δc were determined from the distributions of a, b and c by using 1σ standard intervals. To obtain estimates independent of the 'fitting scale', we divided δa, δb and δc by the 'true' coefficients of the FP, a_t, b_t and c_t, derived from a simulation of large size. In Fig. 4 we plot $\delta a/a_t$, $\delta b/b_t$ and $\delta c/c_t$ against the logarithm of the sample size N for the various MIST fits. To allow a direct comparison with Fig. 2 the same range of N has been plotted.

It is apparent that the true intervals depend on the fitting method and that the most effective fit (i.e. lower values of $\delta a/a$ and $\delta b/b$ for fixed N) is the $\mathrm{MIST}_{\mathrm{BIS}}$ method, in agreement with what found by IFA90 for the bisector line. The largest variances are obtained for the $\mathrm{MIST}_{\log \sigma_0}$ fit. It is also worth to notice that, by changing the scatter along the σ_0 direction in the simulations, the curves shown in the figure undergo just a

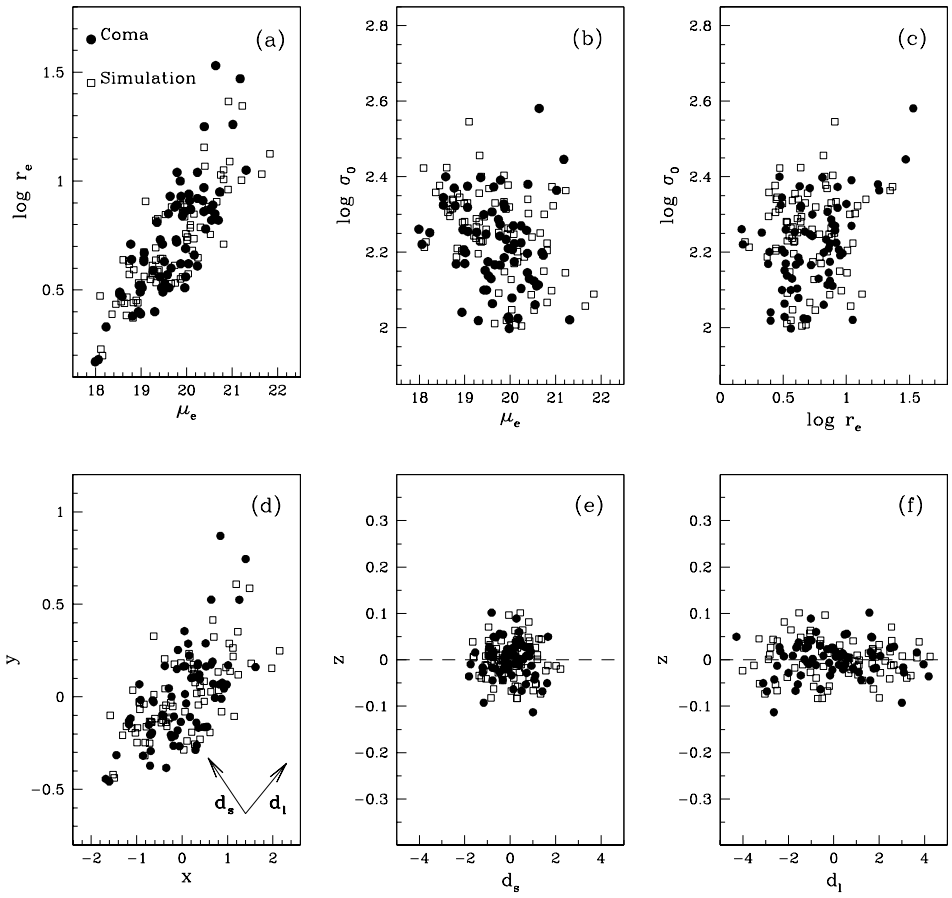

Fig. 3a–f. Comparison of one of the FP simulations with the template sample. **a** Simulation and the Coma photometric sample in the plane $(\mu_{\rm e}, \log {\rm r_e})$. **b** Distribution in the plane $(\mu_{\rm e}, \log \sigma_0)$. **c** Distribution in the plane $(\log {\rm r_e}, \log \sigma_0)$. **d** Face-on view of the FP. **e**, **f** Long and short edge-on views of the FP. The plotted simulation has the same size as the Coma sample.

translation in the y direction, without any change in shape. In the case shown in Fig. 4 we adopted the MV of the rms of $\log \sigma_0$ residuals of various clusters of galaxies (see Sect. 4).

Fig. 4 can be used as a ready tool to state the number of galaxies necessary to achieve a given accuracy on the FP.

Concerning the zero point of the FP, it is important to remark that the uncertainties plotted in Fig. 4 do not represent the estimates of usual interest. For all the applications of the FP zero point (i.e. distance determinations, constraining of cosmological and evolution parameters), the uncertainties on c are derived with the hypothesis that the FP slopes are exactly determined. The errors on c are then given as $1/\sqrt{N}$ multiplied by the rms of the dependent variable residuals. Such estimates are generally smaller than $\delta c/c_t$.

For this reason, in the following we will focus our analysis on the uncertainties of the FP slopes.

Although the comparison of Figs. 2 and 4 does not show an evident disagreement, for $\log N \widetilde{<} 1.8$ ($N \widetilde{<} 60$) the values reported in literature appear almost as a scatter diagram. Starting from this remark, we now analyze the performances of the different methods used to estimate the uncertainties.

3.2.1. Theoretical methods

Although statistics allows to prove the asymptotic validity of variance estimators, it does not furnish an estimate of the 'mini-

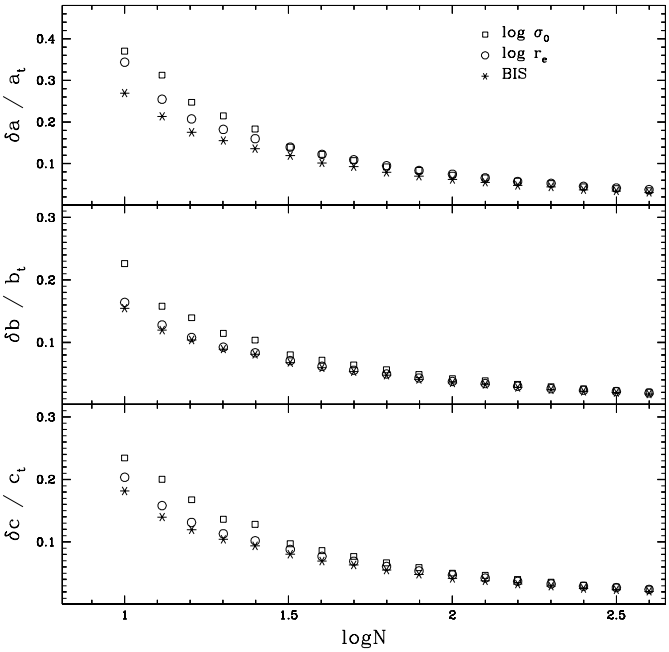

Fig. 4. 'True relative uncertainties' on the FP coefficients against the logarithm of the sample size N. The various MIST fits are plotted by different symbols as shown in the upper right-hand corner. The $\rm MIST_{\log r_e}$ and $\rm MIST_{\mu_e}$ fits are completely consistent, so that for clarity only the first one is plotted. The axes scales are the same as in Fig. 2.

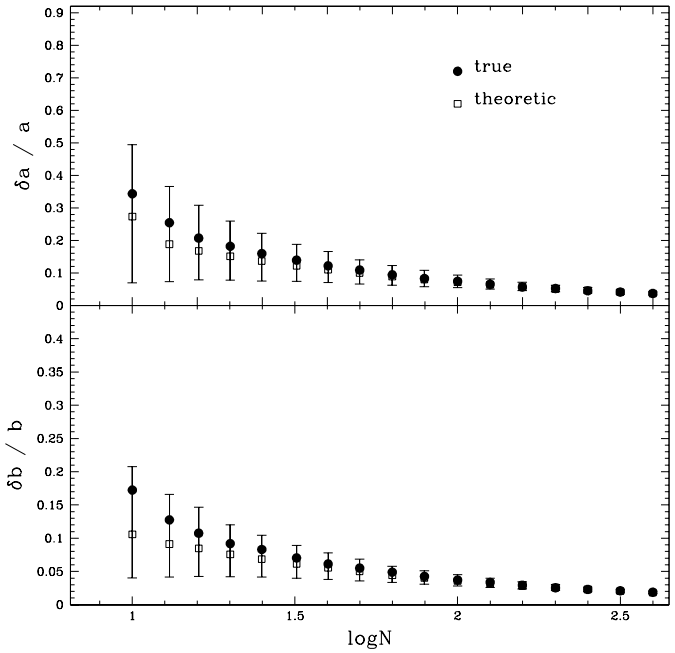

Fig. 5. Comparison of theoretic and true relative uncertainties on the FP slopes (see text). The different symbols are explained in the upper right-hand corner. We adopted the $\mathrm{MIST}_{\log r_e}$ fit.

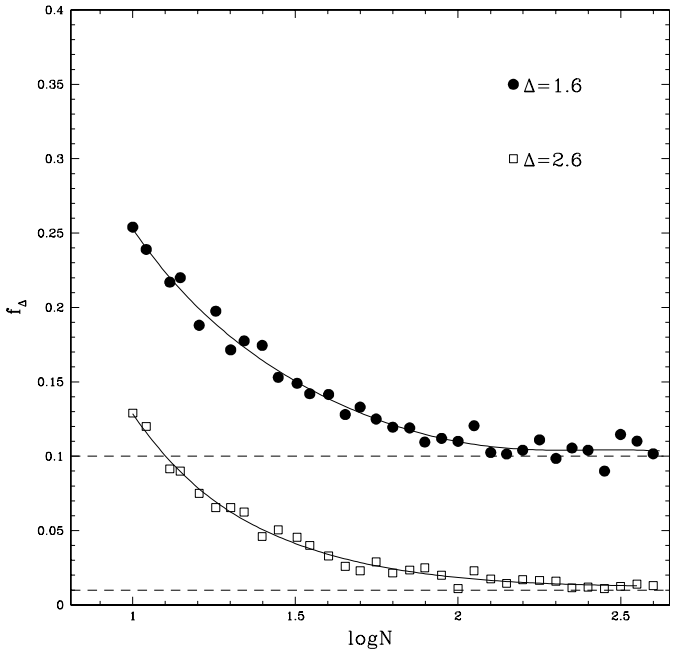

Fig. 6. Fraction of non-consistent simulations, f_Δ, against the sample size N (see text). Circles and rectangles correspond to different values of Δ as shown in the upper right-hand corner. The solid lines were obtained by interpolation. The dashed lines show the asymptotic values of the curves.

mum sample size' for the theoretical formulae to be valid. Since such an estimate will generally depend on the 'shape' of the parent population, it should be obtained each time by using simulation methods.

To test the performance of theoretical variance estimators for the FP coefficients we apply the results of Sect. 2. FP simulations of fixed size N were constructed and theoretical relative uncertainties (1σ standard intervals) on a and b derived for each sample by Eqs. (B17, 10 – 16). In Fig. 5, the MVs of the theoretical estimates, $\delta a/a$ and $\delta b/b$, with corresponding 'error bars', are plotted against the logarithm of N. The error bars were obtained by connecting the 5th and 95th percentiles[6] of the $\delta a/a$ and $\delta b/b$ distributions. For comparison, we also plot the 'true uncertainties' on the slopes as derived from the simulations. As expected, the larger the sample size, the better it is the agreement between theoretical and actual values. For sample sizes smaller than $N_{\min} \approx 30$ ($\log N_{\min} = 1.5$), we see however that theoretical formulae (I) largely scatter (up to 40% for a and 15% for b) and (II) increasingly underestimate the 'true' values (see also IFA90 and Feigelson & Babu 1992).

To discuss in more detail the point II, we calculated for each sample the coefficient a, the theoretical uncertainty δa, and the 'discrepancy' $d_a = |a - a_{\rm t}|/\delta a$, where the actual value, $a_{\rm t}$, of the coefficient a was derived by fitting a simulation of large size. We then determined the fraction of simulations, f_Δ, with d_a greater than a fixed value Δ. The calculation was iterated by varying the sample size.

[6] The pth percentile of a given distribution is the point that exceeds (100-p) ascending order (see e.g. Beers et al. 1990).

In Fig. 6, we plot f_Δ against $\log N$ for two different values of Δ. We chose $\Delta = 1.6$ that, for a normal distribution, defines a confidence level (CL) of 10%, and $\Delta = 2.6$, corresponding to a 1% CL. If Eqs. (14 – 16) worked well, on the average, for every value of N, the fraction of not-consistent samples would be independent of N and determined by the CL corresponding to the value of Δ. Fig. 6 shows that for $N > N_{\min} \approx 30$ ($\log N_{\min} \approx 1.5$) f_Δ is in good agreement (within $\sim$5%) with the expected CLs. For sample sizes smaller than $N_{\min}$, the theoretical formulae do not furnish reliable estimates of the desired CLs: the curves of Fig. 6 increase steeply. The same result was obtained for the coefficient b, and by varying the MIST fit. We also found that the estimate of $N_{\min}$ is largely independent of the simulation parameters: the same estimate was obtained using the FP coefficients and the $\log \sigma_0$ dispersion of the samples studied in Sect. 4.

Fig. 6 suggests that in order to obtain a given confidence level, the uncertainties on the FP coefficients of small samples should be estimated using a σ interval dependent on N. For instance, to obtain a 10% CL with $N = 12$ ($\log N = 1.1$), an effective interval of 2.6σ should be used. However, it turns out that the smaller the sample size with respect to $N_{\min}$, the stronger is the dependence of f_Δ on the adopted fitting method and, what is more critical, on the simulation parameters. For instance, the fraction of not-consistent samples with $N = 10$ varies by $\sim 6\%$ by varying the $\log \sigma_0$ scatter in the simulations.

We conclude that for $N \lesssim 30$ the theoretical formulae are not reliable. Although the desired confidence intervals can be roughly obtained by using effective, suitably tested, standard

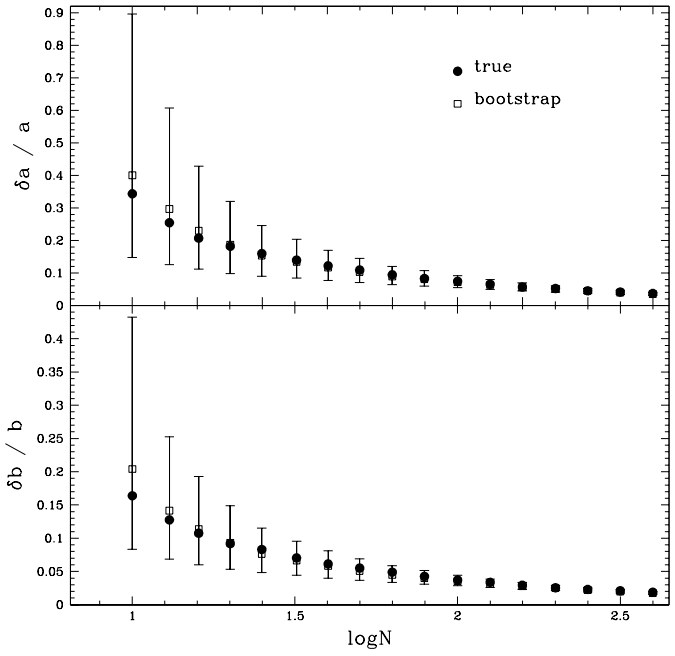

Fig. 7. Comparison of 'bootstrap' and 'true' relative uncertainties on the FP slopes (see text). Different symbols have been used as indicated in the upper right-hand corner. We adopted the $\mathrm{MIST}_{\log r_\mathrm{e}}$ fit. The axes scales are the same of Fig. 5.

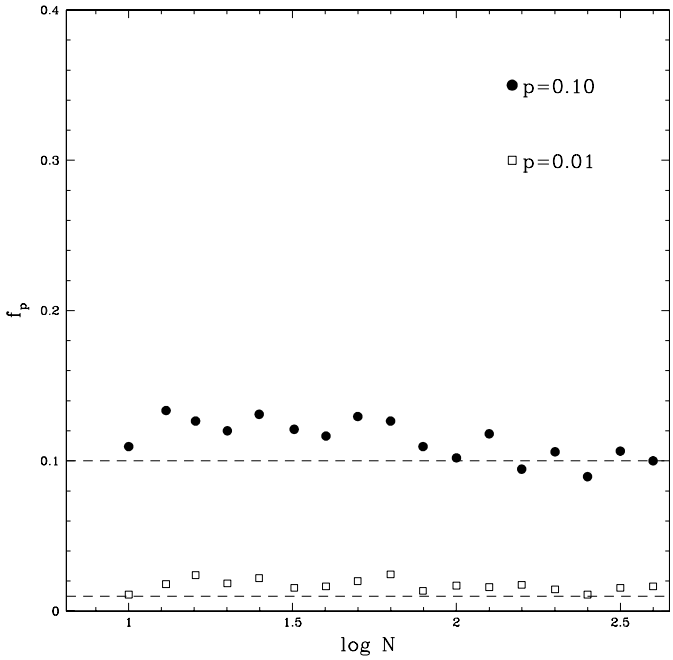

Fig. 8. Fraction of non-consistent simulations, $\mathrm{f_p}$, against $\log N$ (see text). The plot is referred to the coefficient b. Circles and rectangles correspond to $100p\%$ percentile intervals with $\mathrm{p} = 0.10$ and $\mathrm{p} = 0.01$ (see upper right-hand corner). The dashed lines show the desired CLs. The axes scales are the same as in Fig. 6.

intervals, the individual estimates can be significantly different, up to $\sim 20\%$ for a and $\sim 15\%$ for b, with respect to the true values.

3.2.2. Re-sampling procedures

The hypothesis underlying the use of re-sampling methods is that the available data set furnishes a good approximation to the parent population. The statistics of interest is calculated for various pseudo-samples drawn from the actual data set. If this 'sampling hypothesis' holds, the distribution of pseudo-values coincides with the 'true' one and the confidence intervals can be accurately estimated at the cost of some computing time (see e.g. Efron & Tibshirani 1986). However, the smaller the sample size, the larger is the probability that the actual sample gives a poor representation of the parent population. In order to derive a 'minimum sample size' for the re-sampling methods to be reliable, numerical simulations have to be employed.

On the basis of the analysis of the previous section, we studied the performance of re-sampling uncertainties on the FP coefficients by testing the use of the bootstrap method. The results that follow were found to be largely independent of the simulation parameters, of the actual FP coefficients, and of the fitting method.

FP simulations of fixed size N were constructed. For each sample, we determined the FP slopes and the bootstrap uncertainties δa and δb by using 1σ standard intervals with $N_\mathrm{r} = 2000$ pseudo-samples (by further increasing N_r the following results do not change). In Fig. 7, the MVs of the bootstrap relative uncertainties, $\delta a/a$ and $\delta b/b$, with corresponding error bars (see Sect. 3.2.1), are plotted against the logarithm of the sample size and compared to the true values. The error bars are given by 10% percentile intervals[7].

As shown in the figure, the bootstrap method gives a good measure of the average uncertainties, but a very poor, largely scattered, representation of the actual errors.

Only for $N \widetilde{<} 15$ ($\log N \widetilde{<} 1.1$–1.2) the MVs of the re-sampling standard errors appear to differ from the true uncertainties. As a matter of fact, it turns out that this difference is due to the use of 1σ standard intervals to estimate the bootstrap confidence intervals. For small samples, in fact, the distribution of pseudo-values is significantly different from a normal one, so that the desired CLs must be obtained by non-parametric estimates[8] (see Efron & Tibshirani 1986 and Efron 1987). To illustrate this point, we tested the use of bootstrap percentile intervals proceeding as in the previous section (Fig. 6). For each sample size, we derived the fraction of simulations, f_p, that are not consistent with the 'true' FP slopes. The calculation was iterated by adopting different percentile intervals of the pseudo-values. To have a direct comparison with Fig. 6 we chose $100 \cdot p\%$ intervals with $p = 0.10$ and $p = 0.01$ respectively. In Fig. 8, the fraction of non-consistent samples is plotted against the logarithm of the sample size. It turns out that, on the average, the bootstrap

[7] A $p\%$ percentile interval is given by the difference between the $p/2$th and the $(100 - p/2)$th percentiles (see note 6) of the distribution of interest.

[8] I.e. by confidence intervals independent of any assumption on the shape of the probability density of the statistics of interest.

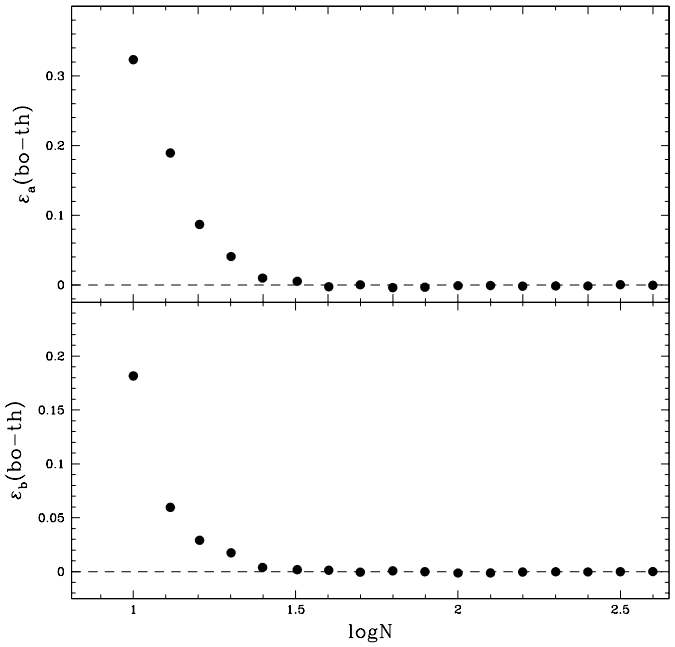

Fig. 9. Differences, $\varepsilon_a(bo-th)$ and $\varepsilon_b(bo-th)$, of the 'scatters' of bootstrap and theoretic uncertainties on a and b, against $\log N$.

allows to give very accurate estimates of the true intervals. For every sample size, differences of only some percents are found with respect to the desired CLs.

On the other hand, by looking at Fig. 7, we notice that for small samples the bootstrap uncertainties have a very large dispersion with respect to true values. The scatter varies from $\sim 5\%$ for $N = N_{\rm min} \approx 30$ up to 60% for $N \approx 10$. Below $N \approx N_{\rm min}$ the FP parent population is poorly represented, so that the single bootstrap estimates can be very unsatisfactory.

To have a comparison with the theoretical methods, we compared the width of the error bars shown in Figs. 5 and 7. In Fig. 9 we plot the difference of the error bars against the logarithm of the sample size.

While for large samples theoretic and bootstrap uncertainties have a similar scatter, for $N \widetilde{<} N_{\rm min} \approx 30$ ($\log N_{\rm min} \widetilde{<} 1.5$) the bootstrap errors become increasingly less accurate. For $N \approx 10$, the scatter increases up to $\sim 30\%$ for a and to $\sim 20\%$ for b.

The conclusions are thus the following.

For large samples, both theoretic and bootstrap methods give accurate estimates of the uncertainties.

For $N \widetilde{<} 30$, both methods give estimates that can differ significantly from the true values. The bootstrap is accurate on the average but the uncertainties have a very large scatter. The theoretical methods give values that are more precise, but systematically underestimated.

4. An application: the FP of cluster galaxies

The use of the FP as distance indicator is based on the hypothesis that its slopes and thickness are 'universal', i.e., independent of the sample of galaxies.

The problem of the universality has been studied by JFK96 by deriving the FPs of ten clusters of galaxies. Although the authors find that the FP coefficients are no significantly different from cluster to cluster, they admit that the samples are too small to get an accurate comparison.

Up to now, the FP has been derived with a significant number of galaxies only for Coma cluster ($N = 81$). Most of the other cluster samples have $N \widetilde{<} 20$–30 (e.g. Dressler et al. 1987, JFK96, Hudson et al. 1997, Pahre et al. 1998).

On the basis of the discussion in Sects. 2 and 3, we try now to address the question of the universality by comparing the FPs of different clusters.

We chose the samples so that a) their size was as large as possible; b) the FP parameters of the different samples were homogeneous; c) each sample had photometric parameters in the same waveband and d) the cluster were at $z \sim 0$. The four prescriptions are needed to a), b) make significant comparisons, c) avoid waveband dependencies, and d) avoid galaxy evolution effects. The ten samples surviving the above criteria are listed in Table 2.

The FP parameters, $\log \sigma_0$, $\log r_{\rm e}$ and $\mu_{\rm e}$ were drawn from literature. The photometry is in Gunn r for JFK data and in Kron-Cousins R band for the other samples. For the present study, the differences of the two wavebands can be completely neglected (see Pahre et al. 1998 and Scodeggio et al. 1998). Only galaxies with $\sigma_0 \geq 95\,{\rm km\,s^{-1}}$ were considered (see e.g. Dressler et al. 1987).

The FP coefficients were determined by the ${\rm MIST}_{\log r_{\rm e}}$, ${\rm MIST}_{\mu_{\rm e}}$, ${\rm MIST}_{\log \sigma_0}$ and ${\rm MIST}_{\rm BIS}$ fits (see Sect. 2.1), by taking into account the measurement errors on the variables as described in Sect. 2.2.

To compare the FP slopes, it should be taken into account that the uncertainties on a and b can be correlated. By Eqs. B17, we obtained the theoretical estimates of the CM components of the slopes. These estimates were then used to derive the ellipse that defines a 10% CL for a normal bi-variate. This is accounted for in Fig. 10.

The Fig. 10 has the disadvantage to be not easily readable. To obtain a more immediate description we compared separately the a and b values as derived from different fits, as plotted in Fig. 11. The FP slopes of the ${\rm MIST}_{\log r_{\rm e}}$ and ${\rm MIST}_{\log \sigma_0}$ fits are also listed in Table 2.

All the samples (except one) have small size, $N \leq N_{\rm min} \approx 30$, so that, as discussed in Sect. 3.2, an accurate estimate of the uncertainties on a and b is not achievable. Approximate error bars were derived by theoretic formulae (Eqs. B17), with the prescriptions of Sect. 3.2.1 to obtain a 10% CL. Since half of the clusters have $N \widetilde{<} 20$, effective theoretic intervals should in fact be more suitable than re-sampling estimates (see Sect. 3.2.2).

Although the coefficients a and b are consistent for each pair of samples in every fitting procedure, we see that the error bars are very large, typically $40\% - 50\%$ of the a and b values. Moreover, they could not represent reliable estimates.

It is also worth to notice that in the ${\rm MIST}_{\log r_{\rm e}}$, ${\rm MIST}_{\mu_{\rm e}}$ and ${\rm MIST}_{\rm BIS}$ fits, the coefficient a of the largest sample (the Coma cluster) is systematically higher with respect to the other

Table 2. Column 1: cluster identification. Column 2: CMB-frame redshift. Column 3: limiting apparent magnitudes. The values were referred to the distance of Coma by using the redshifts of Column 2. Column 4: number of galaxies (E+S0). Column 5: references from which the FP parameters are drawn. Columns 6, 7: FP slopes, a and b, obtained by the $\mathrm{MIST}_{\log r_e}$ fit, with 1σ standard intervals. Columns 8, 9: FP slopes and relative uncertainites (1σ standard intervals) as derived by the $\mathrm{MIST}_{\log \sigma_0}$ method. Column 10: intrinsic dispersion of the FP, $\mathrm{s}_{\log \sigma_0}$, projected along the $\log \sigma_0$ direction. The values were obtained by the $\mathrm{MIST}_{\log \sigma_0}$ fit.

Id.	cz $(\mathrm{km\,s^{-1}})$	m_l	N	Ref.	a	b	a	b	$\mathrm{s}_{\log \sigma_0}$
S639	6545	14.9	12	JFK95a,b	1.14 ± 0.20	0.306 ± 0.033	1.49 ± 0.25	0.300 ± 0.043	0.058
J8	9800	13.8	13	SLH97	0.77 ± 0.24	0.317 ± 0.022	1.38 ± 0.26	0.330 ± 0.040	0.070
A3381	11472	14.8	14	JFK95a,b	1.10 ± 0.13	0.249 ± 0.028	1.50 ± 0.26	0.232 ± 0.026	0.057
S753	4421	14.7	16	JFK95a,b	0.89 ± 0.16	0.341 ± 0.020	1.21 ± 0.16	0.353 ± 0.021	0.061
HYDRA	4050	15.1	18	JFK95a,b	1.19 ± 0.14	0.320 ± 0.028	1.90 ± 0.45	0.316 ± 0.033	0.062
A194	5038	14.7	21	JFK95a,b	0.94 ± 0.12	0.348 ± 0.025	1.26 ± 0.13	0.344 ± 0.025	0.058
PISCES	4700	15.5	24	SLH97	1.16 ± 0.09	0.348 ± 0.037	1.52 ± 0.31	0.348 ± 0.040	0.056
A539	8734	14.9	25	JFK95a,b	1.15 ± 0.12	0.317 ± 0.014	1.51 ± 0.23	0.327 ± 0.018	0.029
PERSEUS	4800	15.1	30	SLH97	1.32 ± 0.18	0.348 ± 0.014	1.68 ± 0.17	0.370 ± 0.017	0.010
COMA	7200	15.4	75	JFK95a,b	1.34 ± 0.07	0.326 ± 0.012	1.53 ± 0.08	0.328 ± 0.013	0.015

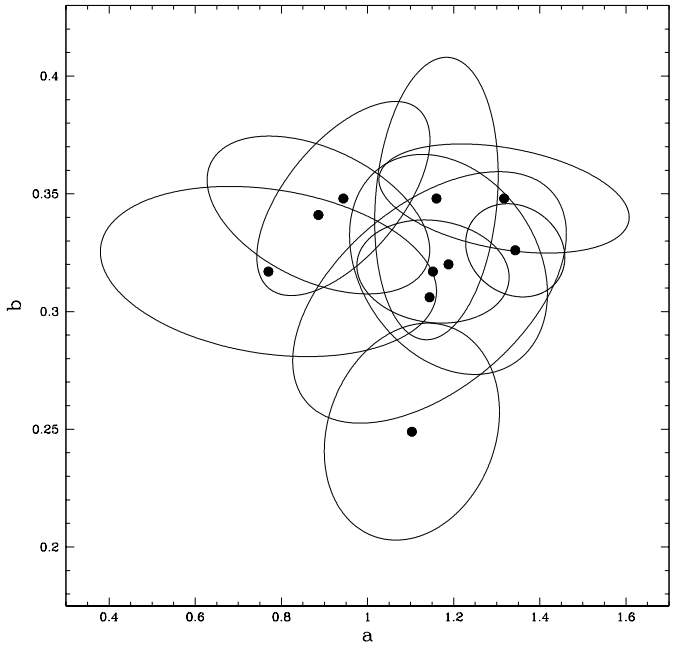

Fig. 10. FP slopes, a and b, of the samples listed in Table 2. The ellipses define a 10% CL. The coefficients were derived by the $\mathrm{MIST}_{\log r_e}$ fit.

determinations. A weak correlation between a and the sample size seems also to be present.

To address this point, we tried to correct the FP slopes for the different magnitude-completeness of the samples (see Giovanelli et al. 1997 and Scodeggio et al. 1998 for a wide discussion). At first, we constructed the completeness histograms of each sample. To this aim, the magnitude range was binned and the fraction of galaxies of each bin normalised to the corresponding fraction of the Coma photometric sample of JFK95a. This data set is complete in fact out to a magnitude higher than the magnitude limits of the other samples (see Table 2 and references therein). It turns out that the same results are also obtained by normalizing the fractions of galaxies through a gaussian model of the luminosity function (see Scodeggio et al. 1998). The histograms were then modeled by Fermi-Dirac distributions and incomplete FP simulations constructed through the modeled distributions. By fitting the simulations, we estimated the corrections on a and b.

As shown in Fig. 11, the corrections shift upwards the coefficient a and reduce the correlation with the sample size and the systematic difference of the Coma sample. It turns out, in fact, that these effects are a consequence of the different completeness of the samples with respect to the photometric parameters. This is shown by the results of the 'inverse' fit, with $\log \sigma_0$ as the dependent variable, that should be less sensitive to the photometric completeness (see Hudson et al. 1997, hereafter HLS97). By looking at Fig. 11, we see that in the $\mathrm{MIST}_{\log \sigma_0}$ method there is no systematic difference between Coma and the other samples.

It is also evident that a systematic difference is present between the FP coefficients derived from the various MIST fits. As discussed in Sect. 2.2, the 'fitting bias' is due to the lack of a model for the intrinsic scatter of the FP. For the same reason, only the projection of the intrinsic dispersion along some assigned direction, with respect to a given fitted plane, can be measured.

For instance, we calculate the scatter projection on the $\log \sigma_0$ variable for $\mathrm{MIST}_{\log \sigma_0}$ fit. For each sample we derived the rms of the $\log \sigma_0$ residuals. The amount of scatter due to the measurement errors was then subtracted in quadrature. The measurement error scatter projected on σ_0 was found to be $\sim 10\%$. By constructing FP simulations with $\sigma_0 \geq 100$, the 'intrinsic rms values' were corrected for the bias due to the $\log \sigma_0$ cut on the cluster samples. The correction was found to be very small (~ 2 – 3%) and largely independent of the simulation parameters.

The $\log \sigma_0$ dispersions are shown in Table 2. The mean values of the $\log \sigma_0$ intrinsic scatter amounts to ~ 0.048, that corresponds to $\sim 10\%$ in σ_0.

In Table 3, we show the weighted means of the coefficients a and b for the various fitting methods. The means were calculated after the magnitude-completeness and the $\log \sigma_0$ corrections.

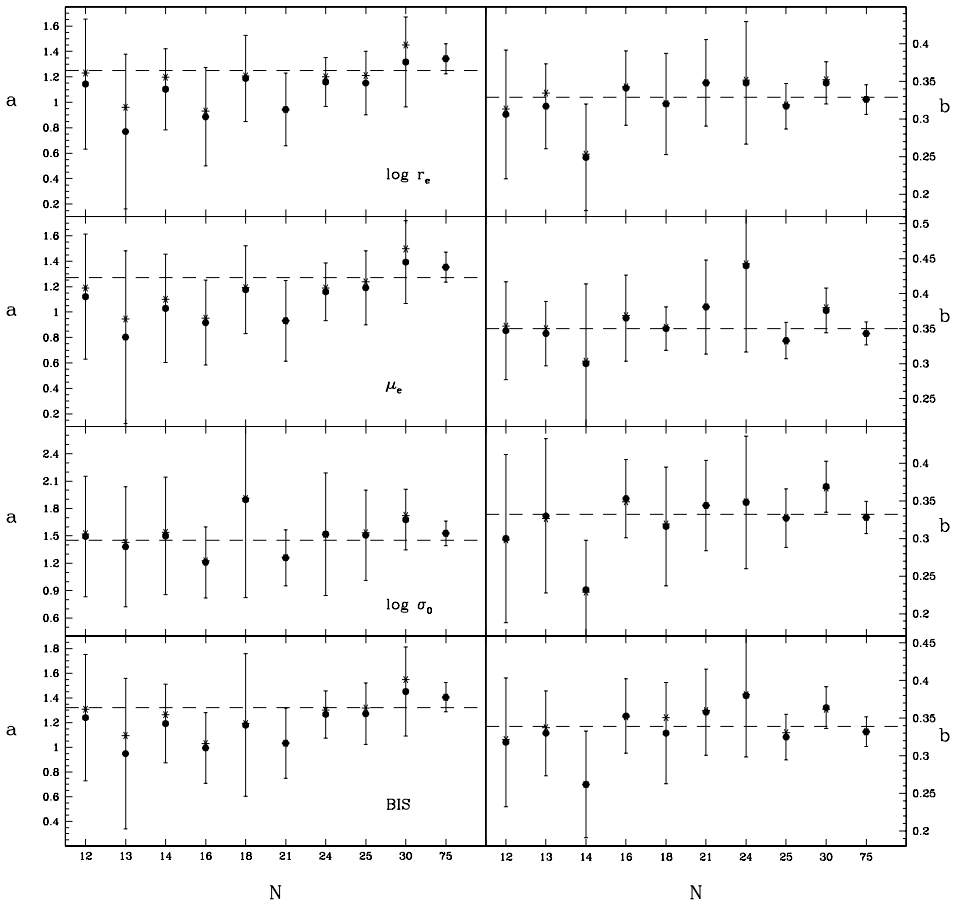

Fig. 11. FP slopes of the clusters listed in Table 2. The coefficients a and b of the different MIST fits are plotted on horizontal panels. The fitting methods are indicated shortly in the lower right-hand corners of the panels on the left. The sample size increases from the left to the right of each panel as shown on the x-axes of the lower panels. The error bars define a 10% CL. The values of a and b after the magnitude-completeness corrections are also plotted by asterisks. The dashed lines correspond to the weighted means of the slopes.

Table 3. Weighted means of the 'corrected' FP slopes (see text). Column 1: fitting method. Columns 2 and 3: mean values of a and b with corresponding uncertainties (1σ intervals).

	$\overline{a}$	$\overline{b}$
$\mathrm{MIST}_{\log r_\mathrm{e}}$	1.25 ± 0.05	0.329 ± 0.008
$\mathrm{MIST}_{\mu_\mathrm{e}}$	1.27 ± 0.05	0.350 ± 0.007
$\mathrm{MIST}_{\log \sigma_0}$	1.45 ± 0.06	0.332 ± 0.009
$\mathrm{MIST}_{\mathrm{BIS}}$	1.32 ± 0.04	0.339 ± 0.007

The $\log \sigma_0$ bias on the slopes of the $\mathrm{MIST}_{\log \sigma_0}$ fit was estimated from the simulations (see above). It amounts to $\sim 5\%$ for a and is completely negligible for b.

The difference between the various MIST fits amounts to $\sim 15\%$ for the coefficient a and to $\sim 6\%$ for b. The coefficient a varies from 1.25 to 1.45, and b from 0.33 to 0.35.

The bias that could be introduced by neglecting the measurement errors was found to be negligible for b ($\widetilde{<}1\%$). Concerning the coefficient a, the bias depends on the fitting procedure: it amounts to $\sim 5\%$ for the $\mathrm{MIST}_{\log r_\mathrm{e}}$ and $\mathrm{MIST}_{\mu_\mathrm{e}}$ methods (in agreement with the estimate given by JFK96), and to $\sim 1\%$ and ~ 3 – 4% for the $\mathrm{MIST}_{\log \sigma_0}$ and $\mathrm{MIST}_{\mathrm{BIS}}$ fits. Because of the correlation between the uncertainties on $\log r_\mathrm{e}$ and μ_e, it turns out that the $\mathrm{MIST}_{\log \sigma_0}$ method is quite insensitive to the uncertainties on the FP parameters.

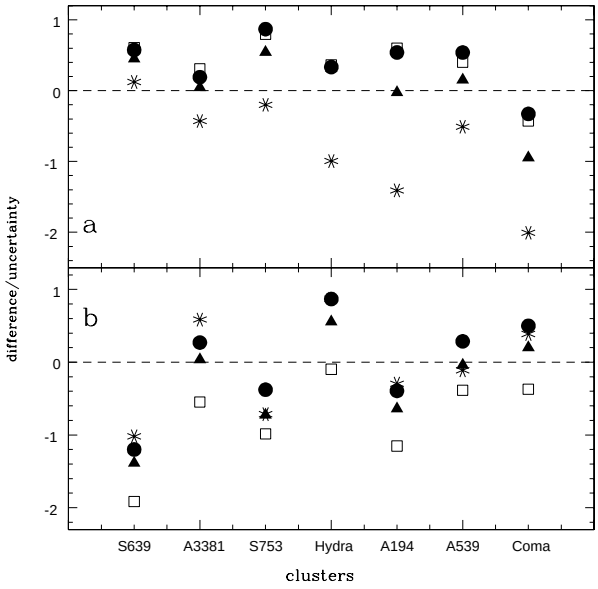

Fig. 12. Comparison of the FP slopes obtained by the MIST fits with the values of JFK96 (see text). Symbols for the different MIST fits are as in Fig. 1.

For what concerns the covariance term of the photometric parameters, as discussed in Sect. 2.2, it was estimated by the relation $\mathrm{C}(\log r_\mathrm{e}, \mu_\mathrm{e}) \approx \alpha \cdot \mathrm{V}(\mu_e)$ with $\alpha \approx 0.30$ (see JFK95a).

By analyzing the correlation of the errors on $\log r_{\rm e}$ and $\mu_{\rm e}$ for various photometric data set drawn from literature, we obtained values of α included between 0.26 and 0.34. Varying α in this range for the calculation of $\rm C(\log r_{\rm e}, \mu_{\rm e})$, very small variations ($< 1\%$) were obtained in the FP coefficients. The higher systematic difference, $\sim 2-3\%$, was found for the coefficient a in the $\log \sigma_0$ fit.

The systematic dependence of the FP coefficients from the fitting method can also be seen by comparing the values obtained by the MIST fits with the results of JFK96 and HLS97.

In Fig. 12 the MIST estimates of a and b are compared to the values of JFK96, that adopted an ORLS (robust) method. To this aim, we plot the differences of the FP slopes (JFK96 $-$ ours) divided by the relative 1σ uncertaintities added in quadrature. The values obtained by JFK96 appear to be consistent with our estimates for each cluster. However, some systematic difference exists. The values of a obtained by the $\rm MIST_{\log r_{\rm e}}$ and $\rm MIST_{\mu_{\rm e}}$ fits are systematically lower than those of JFK96. A small systematic difference is also found for the $\rm MIST_{BIS}$ method. For the $\log \sigma_0$ fit the MIST estimates are systematically higher.

The values of b agree with those by JFK96 for the $\rm MIST_{\log r_{\rm e}}$, $\rm MIST_{\mu_{\rm e}}$ and the $\rm MIST_{BIS}$ methods. On the other hand, the values of the $\rm MIST_{\mu_{\rm e}}$ fit are systematically higher.

The values of the FP slopes obtained by JFK96 for the whole cluster sample, $a = 1.24 \pm 0.07$ and $b = 0.328 \pm 0.008$, are generally consistent with the mean values reported in Table 3. However, systematic differences are particularly evident for the value of a in the $\rm MIST_{\log \sigma_0}$ fit and for the value of b in the $\rm MIST_{\mu_{\rm e}}$ method.

HLS97 derive the FP slopes for a sample of seven clusters of galaxies. By adopting the $\rm OLS_{\log \sigma_0}$ method on all the clusters simultaneously, they obtain $a = 1.383 \pm 0.04$ and $b = 0.326 \pm 0.011$. These values are consistent with the mean values of the $\rm MIST_{\log \sigma_0}$ fit (see Table 3).

The slopes of the individual clusters of HLS97 are derived by a bi-dimensional fit, adopting as independent variable the combination of $\log r_{\rm e}$ and $\mu_{\rm e}$ obtained from the global fit. A direct comparison of our estimates with the individual results of HLS97 is thus not possible.

Since the ORLS and OLS methods do not account for the measurement errors, and due to differences in completeness and selection, a detailed explanation of the origin of the above discrepancies is not achievable.

5. Summary and conclusions

The FP of cluster galaxies is one of the most promising tools to study galaxy evolution, to constrain the epoch of galaxy formation, and to set constraints on the geometry of the universe. To those aims the FP has been recently studied in intermediate-redshift ($z = 0.18$–0.83) clusters (van Dokkum & Franx 1996, Kelson et al. 1997, Bender et al. 1998, van Dokkum et al. 1998, Jørgensen et al. 1999, Kelson et al. 2000). The main step in the above applications is the comparison between FP determinations in different clusters, wavebands and redshifts, for which the determination of the FP coefficients and of the relative uncertainties plays a crucial rôle.

The present study aims at clarifying various aspects in the determination of the FP coefficients and uncertainties.

5.1. The problem of fitting the FP

We introduced a statistical model of the FP that takes into account the measurement errors on the variables and the intrinsic scatter. The correlation between measurement uncertainties is also accounted for.

We derived the $\rm MIST_{\it i}$ (*Measurement errors and Intrinsic Scatter Three dimensional*) fitting procedures, where $i = \log r_{\rm e}, \mu_{\rm e}, \log \sigma_0$ is the dependent variable of the fit. A bisector method, $\rm MIST_{BIS}$, is also introduced.

The assumptions under which the MIST procedures give unbiased estimates of the FP coefficients are that the errors and the intrinsic scatter do not depend on the 'location' on the fitting plane (H1), their covariance matrices are known (H2 and H3), and the covariance matrices of the observed quantities are known (H4).

Under these assumptions, the fits give the same coefficients whatever the choice of the dependent variable.

For what concerns the above assumptions, the knowledge of the average measurement errors can be easily introduced in the procedures in order to satisfy H1 and H2, while the problems posed by H4 can be overcome by assuming a normal distribution for the observed quantities.

Assumption H3, on the other hand, cannot be satisfied since we do not have a model for the intrinsic dispersion of the FP variables. We showed that it is precisely the lack of such a model that biases the best-fit coefficients in such a way that their values depend on the choice of the dependent variable and could not coincide with the slopes of the 'true relation'.

5.2. Uncertainties on the FP coefficients

We addressed the problem of the estimate of the uncertainties on the FP coefficients by numerical simulations based on the best sampled FP so far (the Gunn r FP of Coma by JFK96).

The results of the simulations are presented in Fig. 4 in terms of $\delta a/a$ and $\delta b/b$ versus $\log(N)$. This figure can be used to state the sample size needed to achieve a given accuracy for the FP coefficients.

On the basis of the simulations we tested the performances of the methods used to estimate the uncertainties: the theoretical formulae and the bootstrap technique.

We showed that for $N > N_{min} \approx 30$ the theoretical formulae can recover the variances of the FP coefficients within about 5%, while for $N < N_{min}$ the uncertainties are systematic smaller than the true values and, what is more troublesome, are affected by a large scatter.

The bootstrap technique gives, on the average, more accurate estimates than theoretical methods but for small samples the scatter of the individual values is much larger. Again, a minimum

sample size of $N = N_{min} \approx 30$ exists for the bootstrap to give reliable estimates.

5.3. Implications for the use of the FP

As an application of the present study we addressed in Sect. 4 the question of the 'universality' of the FP. The main obstacles are the limited size of the available (homogeneous) samples and their different completeness characteristics.

We find that the slopes of the FP in the ten clusters considered are consistent *within the large uncertainties* (due to the small number of galaxies in most of the samples). We stress that this result should be taken at most as an indication in favor of the universality of the FP and not as an evidence.

With the available data samples it is not possible to settle the question of the universality: to this aim, larger and more homogeneous samples would be needed.

For the application of the FP to the study of galaxy evolution it would be crucial to know the behavior of the slopes as a function of redshift. Pahre et al. (1998) built a model for the FP that predicts a change in slope with redshift: if age contributes to the tilt of the FP, massive galaxies should be much older than the least luminous ones. As a consequence of this 'differential' evolution, the slopes will change with redshift. They predict the change with redshift of the coefficient a of the FP (see their Fig. 10) by adopting two different models for the stellar evolution (Bruzual & Charlot 1998 and Vazdekis et al. 1996). The Bruzual & Charlot models produces a rapid change of a, that should decrease by about 0.15 from z=0 to z$\sim$0.3, namely, 12% of its local value in the Gunn r band.

Recently, Kelson et al. (2000) derived the FP for a cluster at z=0.33 with 30 galaxies. The authors claim that the slopes are fully consistent with those of the local FP (Coma). They derive the FP by the orthogonal fit and give the following uncertainties for the slopes: $\delta a/a$=0.1 and $\delta b/b$=0.11, that are consistent with the values obtained here from the simulations with n=30 (see Fig. 4). These data seem thus to rule out the rapid evolution of a predicted with the Bruzual & Charlot model.

The situation is quite different with the Vazdekis et al. models. At $z = 0.3$ the slope a decreases by only 0.03%. The minimum sample size needed to achieve such a precision at $z = 0.3$ would be $N \approx 300$, which is out of the reach of any possible observation. The situation improves by moving at higher redshifts, where the magnitude of the predicted change of the slopes is larger. For the cluster at z=0.83 studied by van Dokkum et al. (1998), in fact, the situation is by far more promising. To test the predicted change in slope it would be sufficient to determine the FP on $N \approx 40$ galaxies, that is well within the possibility of a 8–10m class telescope in a reasonable number of nights.

Acknowledgements. We thank the referee for carefully reading the manuscript and for helpful suggestions.

Appendix A

From Eq. (3), we write the probability density (hereafter PD) of Y_i as:

$$f_{Y_i}(Y_i)dY_i = \int f_{X_i}(X_i) \cdot f_{\Phi_i}(Y_i - X_i; X_i)dX_i \qquad \text{(A1)}$$

where $f_{Y_i}(y_i)$ and $f_{X_i}(x_i)$ are the PDs of Y_i and X_i, and $f_{\Phi_i}(\phi_i; X_i)d\phi_i$ is the probability that, for a fixed output of X_i, Φ_i is included between ϕ_i and $\phi_i + d\phi_i$. For brevity, we put $\Phi_{\mathrm{m}i} + \Phi_{\mathrm{s}i} = \Phi_i$.

By Eq. (A1) we obtain the following relations:

$$\begin{aligned}
\mathrm{E}(Y_i) &= \int Y_i f_{Y_i}(Y_i)dY_i = \\
&= \int f_{X_i}(X_i) \left[\int Y_i f_{\Phi_i}(Y_i - X_i; X_i)dY_i \right] dX_i = \\
&= \int X_i f_{X_i}(X_i) \left[\int f_{\Phi_i}(\phi_i; X_i)d\phi_i \right] dX_i + \\
&+ \int f_{X_i}(X_i) \left[\int \phi_i f_{\Phi_i}(\phi_i; X_i)d\phi_i \right] dX_i \qquad \text{(A2)}
\end{aligned}$$

$$\begin{aligned}
\mathrm{V}(Y_i) &= \int \left(Y_i^2 - \mathrm{E}(Y_i)^2\right) f_{Y_i}(y_i)dy_i = \\
&= \int \left[x_i^2 - \mathrm{E}(X_i)^2\right] f_{X_i}(X_i) \left[\int f_{\Phi_i}(\phi_i; X_i)d\phi_i \right] dX_i + \\
&+ 2 \int X_i f_{X_i}(X_i) \left[\int \phi_i f_{\Phi_i}(\phi_i; X_i)d\phi_i \right] dX_i \\
&+ \int f_{X_i}(X_i) \left[\int \phi_i^2 f_{\Phi_i}(\phi_i; X_i)d\phi_i \right] dX_i \qquad \text{(A3)}
\end{aligned}$$

By using the normalization of f_{Φ_i} and the hypothesis $\mathrm{E}(\Phi_i) = 0$, from (A2) we obtain Eq. (7). Eq. (8) follows from (A3) with the further hypothesis that Φ_i and $\{X_i\}$ are not correlated ('hypothesis $\mathcal{H}_1$').

If $\mathcal{H}_1$ does not hold, we obtain again Eq. (8) provided that the CM terms of $\{\Phi_{\mathrm{m}i}\}$ and $\{\Phi_{\mathrm{s}i}\}$ are substituted with their expected values with respect to the PDs of $\{X_i\}$.

In a similar way, Eq. (9) can be proved.

Appendix B

Let's start by introducing the following notations:

$$\mathrm{V}_{ij} = \mathrm{C}(\Phi_{\mathrm{m}_i}, \Phi_{\mathrm{m}_j}) + \mathrm{C}(\Phi_{\mathrm{s}_i}, \Phi_{\mathrm{s}_j}) \qquad \text{(B1)}$$

$$\mathrm{C}_{ij} = \mathrm{C}(Y_i, Y_j) \qquad \text{(B2)}$$

$$\Delta = \left[\mathrm{C}_{12} - \mathrm{V}_{12}\right]^2 - \left[\mathrm{C}_{11} - \mathrm{V}_{11}\right]\left[\mathrm{C}_{22} - \mathrm{V}_{22}\right] \qquad \text{(B3)}$$

$$\Delta_1 = \left[\mathrm{C}_{23} - \mathrm{V}_{23}\right]\left[\mathrm{C}_{12} - \mathrm{V}_{12}\right] - \left[\mathrm{C}_{13} - \mathrm{V}_{13}\right]\left[\mathrm{C}_{22} - \mathrm{V}_{22}\right] \qquad \text{(B4)}$$

$$\Delta_2 = \left[\mathrm{C}_{12} - \mathrm{V}_{12}\right]\left[\mathrm{C}_{13} - \mathrm{V}_{13}\right] - \left[\mathrm{C}_{23} - \mathrm{V}_{23}\right]\left[\mathrm{C}_{11} - \mathrm{V}_{11}\right] \qquad \text{(B5)}$$

The symbols $\hat{\Delta}$, $\hat{\Delta_1}$ and $\hat{\Delta_2}$ will indicate the quantities obtained by substituting C_{ij} in Eqs. (B3 – B5) with unbiased estimates $\hat{\mathrm{C}}_{ij}$.

From Eqs. (10 – 13) we have:

$$\hat{\alpha} - \alpha = \left\{ \frac{\hat{\Delta_1}}{\hat{\Delta}} - \frac{\Delta_1}{\Delta} \right\} =$$

$$= \frac{1}{\Delta}\left\{\left(\hat{\Delta}_1 - \Delta_1\right) - \alpha\left(\hat{\Delta} - \Delta\right)\right\} + o \quad \text{(B6)}$$

$$\hat{\beta} - \beta = \frac{1}{\Delta}\left\{\left(\hat{\Delta}_2 - \Delta_2\right) - \beta\left(\hat{\Delta} - \Delta\right)\right\} + o \quad \text{(B7)}$$

where $\hat{\alpha}$ and $\hat{\beta}$ are defined by replacing C_{ij} with $\hat{\mathrm{C}}_{ij}$ in Eqs. (10, 11), and o is a quantity that can be neglected when the sample size increases.

By using the relation

$$\hat{\mathrm{E}}(\Sigma) = \mathrm{E}(\Sigma) + o \quad \text{(B8)}$$

where Σ is a generic RV and $\hat{\mathrm{E}}(\Sigma)$ an unbiased estimate of $\mathrm{E}(\Sigma)$, the following relations can be written:

$$\hat{\mathrm{C}}_{ij} - \mathrm{C}_{ij} = \hat{\mathrm{E}}(Y_iY_j) - \mathrm{E}(Y_iY_j) - \hat{\mathrm{E}}(Y_i)\mathrm{E}(Y_j) + - \mathrm{E}(Y_i)\hat{\mathrm{E}}(Y_j) + o \quad \text{(B9)}$$

$$\begin{aligned}\hat{\mathrm{C}}_{ij}\hat{\mathrm{C}}_{kl} - \mathrm{C}_{ij}\mathrm{C}_{kl} &= \mathrm{C}_{ij}\left\{\left[\hat{\mathrm{E}}(Y_kY_l) - \mathrm{E}(Y_kY_l)\right] + \right.\\ &+ \mathrm{E}(Y_k)\left[\hat{\mathrm{E}}(Y_l) - \mathrm{E}(Y_l)\right] - \mathrm{E}(Y_l)\left[\hat{\mathrm{E}}(Y_k) - \mathrm{E}(Y_k)\right]\Big\} +\\ &+ \mathrm{C}_{kl}\left\{\left[\hat{\mathrm{E}}(Y_iY_j) - \mathrm{E}(Y_iY_j)\right] - \mathrm{E}(Y_i)\left[\hat{\mathrm{E}}(Y_j) - \mathrm{E}(Y_j)\right] + \right.\\ &- \mathrm{E}(Y_j)\left[\hat{\mathrm{E}}(Y_i) - \mathrm{E}(Y_i)\right]\Big\} + o \end{aligned} \quad \text{(B10)}$$

Setting $\mathrm{P}_{ijlk} = (\mathrm{C}_{ij} - \mathrm{V}_{ij})\, Y_lY_k$ and $\mathrm{q}_{ijl} = (\mathrm{C}_{ij} - \mathrm{V}_{ij})\,\mathrm{E}(Y_l)$, we introduce the RVs ζ, ζ_1 and ζ_2 by the following definitions:

$$\zeta\cdot\Delta = 2\mathrm{P}_{1212} - \mathrm{P}_{1122} - \mathrm{P}_{2211} + 2\left[\mathrm{q}_{221} - \mathrm{q}_{122}\right]\mathrm{Y}_1 + + 2\left[\mathrm{q}_{112} - \mathrm{q}_{121}\right]\mathrm{Y}_2 \quad \text{(B11)}$$

$$\zeta_1\cdot\Delta = \mathrm{P}_{2312} + \mathrm{P}_{1223} - \mathrm{P}_{2213} - \mathrm{P}_{1322} + [2\mathrm{q}_{132} - \mathrm{q}_{123} + - \mathrm{q}_{231}]\,\mathrm{Y}_2 + [\mathrm{q}_{223} - \mathrm{q}_{232}]\,\mathrm{Y}_1 + [\mathrm{q}_{221} - \mathrm{q}_{122}]\,\mathrm{Y}_3 \quad \text{(B12)}$$

$$\zeta_2\cdot\Delta = \mathrm{P}_{1312} + \mathrm{P}_{1213} - \mathrm{P}_{1123} - \mathrm{P}_{2311} + [2\mathrm{q}_{231} - \mathrm{q}_{123} + - \mathrm{q}_{132}]\,\mathrm{Y}_1 + [\mathrm{q}_{113} - \mathrm{q}_{131}]\,\mathrm{Y}_2 + [\mathrm{q}_{112} - \mathrm{q}_{121}]\,\mathrm{Y}_3 \quad \text{(B13)}$$

Using Eqs. (B8 – B13) and setting $\zeta_\alpha = \zeta_1 - \alpha\zeta$, $\zeta_\beta = \zeta_2 - \beta\zeta$, after lengthy calculations, Eqs. (B6,B7) are rewritten:

$$\hat{\alpha} - \alpha = \hat{\mathrm{E}}(\zeta_\alpha) - \mathrm{E}(\zeta_\alpha) + o \quad \text{(B14)}$$

$$\hat{\beta} - \beta = \hat{\mathrm{E}}(\zeta_\beta) - \mathrm{E}(\zeta_\beta) + o \quad \text{(B15)}$$

From the above relations and Eq. (12), we also have:

$$\hat{\gamma} - \gamma = \hat{\mathrm{E}}(\zeta_\gamma) - \mathrm{E}(\zeta_\gamma) + o \quad \text{(B16)}$$

where $\zeta_\gamma = Y_3 - \alpha Y_1 - \beta Y_2 - \mathrm{E}(Y_1)\zeta_\alpha - \mathrm{E}(Y_2)\zeta_\beta$.

If $\{Y_i\}$ are normally distributed, estimates of the expected values in the previous equations are given by sample means. The CM terms of α, β and γ are thus obtained by the usual formulae:

$$\hat{\mathrm{C}}(\hat{\mu},\hat{\nu}) = \frac{1}{N(N-1)}\sum_{i=1,N}(\hat{\zeta_{\mu i}} - \overline{\hat{\zeta_\mu}})(\hat{\zeta_{\nu i}} - \overline{\hat{\zeta_\nu}}) \qquad \mu,\nu = \alpha,\beta,\gamma \quad \text{(B17)}$$

where N is the sample size and $\hat{\zeta_\alpha}$, $\hat{\zeta_\beta}$ and $\hat{\zeta_\gamma}$ are the RVs obtained by substituting in the expressions of ζ_α, ζ_β and ζ_γ the unknown quantities with their unbiased estimates.

References

Akritas M.G., Bershady M.A., 1996, ApJ 470, 706
Beers T.C., Flynn K., Gebhardt K., 1990, AJ 100, 32
Bender R., Burstein D., Faber S.M., 1992, ApJ 399, 462
Bender R., Saglia R.P., Ziegler B., et al., 1998, ApJ 493, 529
Bruzual G.A., Charlot S., 1998, ApJ in preparation
Busarello G., Capaccioli M., Capozziello S., et al., 1997, ApJ 320, 415
Ciotti L., Lanzoni B., Renzini A., 1996, MNRAS 282, 1
de Carvalho R.R., Djorgovski S., 1992, ApJ 389, L49
Djorgovski S., Davies M., 1987, ApJ 313, 59
D'Onofrio M., Capaccioli M., Zaggia S., et al., 1997, MNRAS 289, 847
Dressler A., Lynden-Bell D., Burstein D., et al., 1987, ApJ 313, 42
Efron B., 1979, Ann. Statist. 7, 1
Efron B., Tibshirani R.J., 1986, Statist. Science 1, 54
Efron B., 1987, J. Amer. Statist. Assoc. 82, 171
Faber S.M., Dressler A., Davies L.R., et al., 1987, In: Faber S.M. (ed.) Nearly Normal Galaxies.1 Springer Verlag, New York, p. 175
Feigelson E.D., Babu G.J., 1992, ApJ 397, 55
Giovanelli R., Haynes M.P., Herter T., et al., 1997, AJ 113, 22
Graham A.W., Colless M., 1996, MNRAS 287, 221
Graham A.W., 1998, MNRAS 295, 933
Hudson M.J., Lucey J.R., Smith R.J., et al., 1997, MNRAS 291, 488
Isobe T., Feigelson E.D., Akritas M.G., et al., 1990, ApJ 364, 104
Jørgensen I., Franx M., Kjærgaard P., 1995(a), MNRAS 273, 1097
Jørgensen I., Franx M., Kjærgaard P., 1995(b), MNRAS 276, 1341
Jørgensen I., Franx M., Kjærgaard P., 1996, MNRAS 280, 167
Jørgensen I., Franx M., Hjorth J., et al., 1999, MNRAS 308, 833
Kjærgaard P., Jørgensen I., Moles M., 1993, ApJ 418, 617
Kelson D.D., van Dokkum P.G., Franx M., et al., 1997, ApJ 478, L13
Kelson D.D., Illingworth G.D., van Dokkum P.G., et al., 2000, ApJ 531, 184
Lucey J.R., Bower R.G., Ellis R.S., 1991, MNRAS 249, 755
Mobasher B., Guzman R., Aragon-Salamanca A., et al., 1999, MNRAS 304, 225
Pahre M.A., Djorgovski S.G., de Carvalho R.R., 1995, ApJ 453, L17
Pahre M.A., de Carvalho R.R., Djorgovski S.G., 1998, AJ 116, 1606
Prugniel P., Simien F., 1994, A&A 282, L1
Prugniel P., Simien F., 1996, A&A 309, 749
Prugniel P., Simien F., 1997, A&A 321, 111
Quenouille M., 1949, J. R. Statist. Soc. B 11, 18
Recillas-Cruz E., Carrasco L., Serrano P.G., et al., 1990, A&A 229, 64
Recillas-Cruz E., Carrasco L., Serrano P.G., et al., 1991, A&A 249, 312
Renzini A., Ciotti L., 1993, ApJ 416, L49
Scodeggio M., Gavazzi G., Belsole E., et al., 1998, MNRAS 301, 1001
Smith R.J., Lucey J.R., Hudson M.J., et al., 1997, MNRAS 291, 461
Tukey J., 1958, Ann. Math. Statist. 29, 614
van Dokkum P.G., Franx M., 1996, MNRAS 281, 985
van Dokkum P.G., Franx M., Kelson D.D., et al., 1998, ApJ 504, L17
Vazdekis A., Casuso E., Peletier R., et al., 1996, ApJS 106, 307
Ziegler B.L., Bender R., 1997, MNRAS 291, 527
Ziegler B.L., Saglia R.P., Bender R., et al., 1999, A&A 346, 13